Nanoindentation unidirectional sliding and lateral force microscopy: Evaluation of experimental techniques to measure friction at the nanoscale

F. G. Echeverrigaray,[1] S. R. Sales de Mello,[1] C. D. Boeira,[1] L. M. Leidens,[1] M. E. H. Maia da Costa,[2] F. L. Freire, Jr.,[2] F. Alvarez,[3] A. F. Michels,[1] and C. A. Figueroa[1,4,a]

[1]*PPGMAT, Universidade de Caxias do Sul, Caxias do Sul 95070-560, Brazil*
[2]*Departamento de Física, Pontifícia Universidade Católica do Rio de Janeiro, Rio de Janeiro - RJ 22453-900, Brazil*
[3]*Instituto de Física "Gleb Wataghin", Universidade Estadual de Campinas, Campinas, SP 13081-970, Brazil*
[4]*Plasmar Tecnologia Ltd., Caxias do Sul 95030-775, Brazil*

(Received 9 July 2018; accepted 19 November 2018; published online 17 December 2018)

Lateral force microscopy (LFM) is an established technique to assess friction forces at the nanoscale. Nanoindentation followed by unidirectional sliding (NUS) is also used to evaluate friction forces at the micro/nanoscale. However, comparative studies between NUS and LFM evaluating the experimental results at different scales are still missing. In this work, a-C:D/H and a-C:H thin films with different [D]/[C] and [H]/[C] contents were used to analyze the friction forces by NUS and LFM. The results show that the friction behavior assessed by these two techniques in different scales is the same. The correlation between friction forces measured by NUS and LFM depends mainly on a contact area factor that makes invariant the friction force from nanoscale to microscale. Such behavior suggests a similar damping mechanism, probably phonon-coupling phenomena, for the friction force origin.
https://doi.org/10.1063/1.5047801

I. INTRODUCTION

Friction forces are complex manifestations of nature. From Leonardo da Vinci's experiments, friction has captivated the attention and curiosity of the scientific community. The simplicity of the coefficient of friction and shear stress contrast to the complexity of friction mechanisms and different contributions that were discovered in the last three decades.[1–3]

From a macroscopic point of view, the friction force is an average effect involving several friction mechanisms.[4] In the case of wear-less friction, elastic and electromagnetic interactions determine friction forces. When a tip is sliding on a surface at low normal loads and neglecting electrostatic contributions, both elastic deformation and van der Waals forces dominate the friction mechanisms. Looking at the atomic scale, the elastic deformation can be associated with phononic mechanisms, i.e., atoms from both surfaces are intimately in contact. Consequently, vibrational motion coupling prompts dissipating energy by linear momentum interchange between the sliding surfaces.[5] In the case of phenomena involving van der Waals forces, this electromagnetic contribution is attractive.[5]

From a statistical point of view, the fluctuation-dissipation theorem (FDT) provides a full description of the phenomena connecting the micro/nanoscopic to macroscopic dissipative forces involved in the friction mechanism.[6] By considering an average phonon energy in a solid, the frequency ν

[a]Corresponding author: cafiguer@ucs.br

of atomic collisions per unit of time is $\nu \sim 10^{13} s^{-1}$.[7] Therefore, the momentum (energy) exchange between sliding surfaces can be assumed in quasi-equilibrium. More specifically, the energy transfer can be considered as taking place from the isothermal bath of two-dimensional quasi-equilibrium system (tip and film) interchanging energy through the interface. In standard experimental conditions, a Δx displacement of the tip at the velocity V, the condition $V/\Delta x << \nu \sim 10^{13}\ s^{-1}$ infers that the energy transfer occurs in quasi-equilibrium conditions. It is very tempting to do a parallel between this analysis and the one leading to Einstein's famous relationship $\mu = D/kT$. Here, μ is the mobility, D is the diffusion constant, k the Boltzmann constant, and T the absolute temperature. This famous expression means that the mobility (proportional to the inverse of the friction constant) is related to the fluctuation of the velocity of the Brownian motion.[6] The chaotic sea of phonons colliding with the sliding tip resembles the Brownian motion and, therefore, it is related to the resistance (friction) opposing to the displacement of the tip. Recently, the dream of measuring the friction force atom-by-atom became real, thus the Brownian motion and the fluctuation-dissipation theorem in the friction phenomena may be tested experimentally.[8]

Lateral force microscopy - LFM (or friction force microscopy - FFM) and quartz-crystal microbalance - QCM are generally used to quantify friction forces at the nanoscale.[3,5] By using LFM/FFM, a tip in contact-mode sliding along a surface is also a tool to measure dissipative forces at the nanoscale.[9,10] As it was recently reported, nanoindentation followed by unidirectional sliding (NUS) is a valuable technique providing information about the phonon energy dissipation mechanism at the nanoscale and microscale friction experiments.[11,12] Nevertheless, due to the difficulties evaluating the plastic deformation of the probed samples with this technique, criticisms to such method could be raised. Indeed, in NUS experiments there are two concomitant size scales involved in the technique that must be specifically considered: the z-axis (depth due to the nano-scale penetration of the tip) and the xy-plane (two-dimension due to the tip micro-scale involving the sample surface). Then, altogether, NUS experiments may potentially induce plastic deformation and prevent a proper determination of friction at the nanoscale.

It is important to remark that these possible criticisms to the NUS technique are mainly based in the lack of conclusive experiments comparing results of friction at the nanoscale obtained in the same set of samples by NUS and LFM techniques. Consequently, to contribute to answer these questions, the aim of this work is ***vis à vis*** to quantitatively evaluate and compare the friction at the nanoscale/microscale obtained by nanoindentation followed by unidirectional sliding (NUS) and lateral force microscopy (LFM) techniques.

II. MATERIAL AND METHODS

We have used two different set of samples for nanotribological experiments reported in this paper. The first set is constituted by deuterated/hydrogenated amorphous carbon films (a-C:D/H) deposited by plasma enhanced chemical vapor deposition technique. The concentration of CD_4 and CH_4 precursors was modified to adjust different D/C ratios. A full description of the deposition process and structural and physicochemical characterizations of such thin films can be found elsewhere.[13] The second set is constituted by hydrogenated amorphous carbon films (a-C:H) that were deposited by pulsed DC-PECVD method assisted by electrostatic plasma confinement.[14] The gaseous concentration mixture of C_2H_2 and H_2 precursors (from 100% and 0% to 10% and 90% of C_2H_2 and H_2, respectively) was adequate to obtain different H/C ratios at the outermost layers of the films.[15] A comprehensive description of the deposition process as well as the structural and physicochemical characterizations of such thin films can be found elsewhere.[16] Table I summarize the deposition conditions of thin films studied in this work.

Tribological testing techniques provide quantitative characterization of friction forces acting at the sliding interface expanding from microscale to nanoscale size. Although nanoscale friction phenomena studied by LFM takes generally place in a wear-less regime, the contribution of plastic deformation mechanisms to friction forces measured by nanoindentation followed by unidirectional sliding experiments is a critical question to carefully taking in account. Indeed, nanoindentation takes place at the nanoscale, nonetheless unidirectional sliding assesses a microscale contact.

TABLE I. Brief description of sample preparation.

Thin film	Details
a-C:H/D[a]	Plasma enhanced chemical vapor deposition (PECVD) by RF power supply (13.56 MHz) on Si (100) substrate, thin film thickness ~400 nm
a-C:H[b]	Pulsed DC-PECVD system assisted by electrostatic confinement of plasma in segmented hollow cathode (SHC) on AISI 4140 carbon steel with SiC_x:H:O adhesion interlayer, thin film thickness ~2.85 μm

[a]See Ref. 11, 13.
[b]See Ref. 14, 15.

The NUS tests were performed using a nano-tribometer (NanoTest-600 model - Micro Materials Ltd.) using a conical diamond tip, 25 μm ending radius. The friction test were performed in one-way sliding mode friction on a-C:D/H and a-C:H thin films. A statistical of five unidirectional sliding trails were performed by using a 10 mN constant tip normal force at a rate of ~1 $\mu m.s^{-1}$. More experimental details can be consulted elsewhere.[11]

Complementary experiments of bidirectional sliding tests at the nanoscale were performed by lateral or friction force microscopy (LFM or FFM). The instrument employed in these experiments is a SPM-9700 model - Shimadzu with a square pyramidal Si_3N_4 tip with nominal ending radius of ~15 nm, mounted on a gold-coated V-shaped cantilever (OMCL-TR800PSA-1, Olympus) and nominal spring constant of ~0.36 N/m. Inside the instrument's chamber, the temperature and relative humidity were kept at (21 ± 1) °C and (55 ± 2)%, respectively. The values of friction forces were calibrated employing the "wedge calibration method", using commercially available gratings, according to the procedure reported in Ref. 17 and obtained from the topographical images with a resolution of 512 x 512 pixels taken at 0.25 Hz scan rate and constant normal force of 43.2 nN.

The effect of the tip indentation and sliding (NUS) on the studied samples were assessed by a field emission scanning electron microscope (FEG-SEM/Tescan, MIRA3 model). The FEG-SEM images were carried out for unidirectional sliding measurements at 10 mN (low) and 500 mN (high) indentation normal forces applied on a-C:D/H thin films.

Mechanical properties such as hardness (H), elastic modulus (E) and reduced elastic modulus (E_r) were determined in a NanoTest-600 equipment by using a Berkovich diamond tip (Micro Materials Ltd.). The initial load applied was 0.1 mN and the maximum displacement does not exceed 100 nm, the loading/unloading rates were 0.1 mN/s, and the dwell time at maximum load was 5 s. At least 15 indentations were performed on each studied thin film. The data were examined using the Oliver and Pharr method[18] with the analytical software provided by Micro Materials. The nanoindentation measurements were used to determine the elastic deformation (H/E ratio) and plastic deformation (H^3/E^2 ratio) indexes as described elsewhere.[19,20]

III. CONTACT MECHANICS THEORY AND CALCULATIONS

Contact mechanic calculations have considered the non-adhesive Hertzian's theory (approximating the surface asperities as spherical "bumps" - termed Hertzian-point contacts),[21,22] the Greenwood and Williamson contact theory (GW model)[23,24] for individual asperities (single asperity contact and continuous contact area) and extended analysis to include frictional sliding.[25] Here, briefly we reproduce the essentials of the GW model. We assume that the mechanical contact is based on a single rigid spherically capped asperity (indenter tip), which approximates as a flat surface (solid lubricant coating) by a random height distribution of asperities and with identical radius of curvature. In such a case, the non-dimensional nominal pressure within the elastic steady state of the material (also is called "shakedown" process) is hemispherically distributed on a plane contact area (area of the spherical zone) with a contact area radius a given by:[25]

$$a = \left(\frac{3NR_r}{4E_r}\right)^{1/3} \tag{1a}$$

The interference δ or overlap between profiles is given by

$$\delta = \frac{a^2}{R_r} = \left(\frac{9N^2}{16R_r E_r^2}\right)^{1/3} \tag{1b}$$

and the mean Hertzian contact pressure ρ is expressed by

$$\rho = \frac{2}{3\pi}\left(\frac{6NE_r^2}{R_r^2}\right)^{1/3} \tag{1c}$$

Here N is the normal force or applied load (in Hertzian contacts, $A \propto N^{2/3}$, for small external loads, the circular contact region is almost proportional to the compressive force, in which only one small-scale asperity is in contact with the counter-face); R_r and E_r are the reduced radius of curvature and reduced modulus, given by $1/R_r = 1/R_x + 1/R_y$ and $1/E_r = (1 - \nu_1/E_1) + (1 - \nu_2/E_2)$, respectively. For circular contact, $R_x = R_y$, ν_i and E_i are the Poisson's ratio and Young's modulus, respectively.

The relation between the real (effective contact) to apparent (nominal contact) area of contact (A_r/A_a) in the elastic regime for asperity junctions as a function of the [D]/[C] and [H]/[C] concentration ratios was obtained for each mechanical system by the equations:[26]

$$A_r = \sum_{i=1}^{n} A_i \sim \frac{3.2NR^{*(1/2)}}{E_r\sigma^{(1/2)}} \tag{2}$$

$$A_i = \pi a_i^2 = f(\delta_i) \tag{3}$$

$$A_a = 2\pi Rh \tag{4}$$

Where A_i is the area of individual contact spots, n the number of contact spots, the function $f(\delta_i)$ depends upon the material properties of the sliding surfaces. By assuming elastic junctions by discrete-random process analysis as used in GW analysis, R^* is the radius (R^* was experimentally determined by AFM in topography mode and its mean value is 60 nm for a-C:D/H and a-C:H thin films) of the spherically capped asperity peaks and R is the nominal contact radius of tip obtained by considering the contact pressure of diamond tip of ~25 μm radius (NUS) and 10% of the effective contact for the Si_3N_4 tip (~15 nm radius - LFM). Finally, σ is the standard deviation of the asperity peak-height distribution or RMS surface roughness and h is the indentation depth. We remark that the fractional contact areas may be at least $\sim 10^{-4}$ and a linear relation between effective areas and applied load up to ~10% must be verified to validate the measurements.[27–29]

The extended GW model proposes a plasticity index in repeat sliding (Ψ_s) which describes the transition from elastic to plastic deformation of surface asperities. This repeat sliding of friction causes blunting and flattening of the spherically capped asperities, strain hardening and residual stresses due to plastic deformation, all of which tend to lead toward an elastic steady state by the asperity shakedown pressure (ρ_s). Thus, the Ψ_s is given by:[23,25]

$$\psi_S = \frac{E_r}{\rho_S}\sqrt{\frac{\sigma}{R^*}} \tag{5}$$

where $\rho_s = \rho$ in case asperities elastically compressed. For $\Psi_s < 0.6$ elastic deformation dominates and if $\Psi_s > 1$ a large proportion of contact will involve plastic deformation. When Ψ_s is within 0.6 to 1 the deformation mode is in doubt.

IV. RESULTS AND DISCUSSION

Figure 1 shows the evolution of friction forces for a-C:D/H thin films having different [D]/[C] concentration ratios and measured by NUS and LFM. Although the absolute values of friction forces are different by five (5) orders of magnitude, the quite similar tendencies are equivalent.

On the one hand, the friction forces obtained by LFM come from the interaction of the 15 nm tip sliding on the outermost nanolayer of the a-C:D/D thin films. On the other hand, the friction forces obtained by NUS are due to the interaction of a 25 μm conical diamond tip μm sliding on a-C:D/H

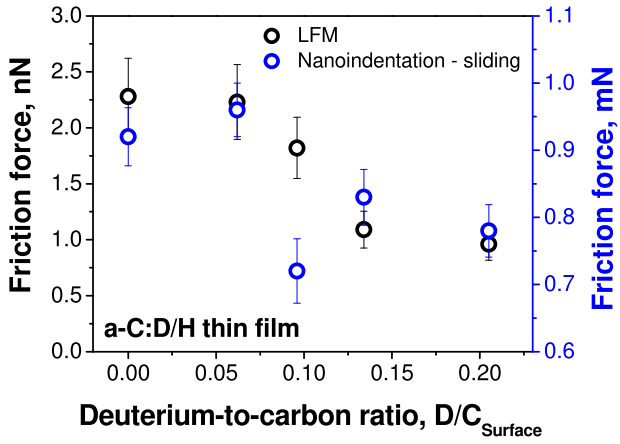

FIG. 1. Friction forces measured by NUS and LFM in a-C:D/H thin films having different [D]/[C] concentration ratios.

thin films at 75 nm penetration depth. For the last, the contact area in the order of micrometers square and the penetration depth justify the friction forces in the order of mN. These equivalent tendencies strongly suggest that the measured friction forces differ by a constant scaling factor and both techniques may be probing the same physical phenomena involving energy dissipation effects.

The main difference between the NUS and LFM measurements is the indentation depth. In the case of the NUS technique, elastic and/or plastic deformation mechanisms may occur. Nevertheless, the state-of-the-art in theoretical and experimental tribology allows analyzing the influence of those phenomena, obtaining valuable information about the friction dissipative forces of the tribological system. It is important to remark, however, that neither hardness nor elastic modulus can be independently used as suitable parameters to determine elastic and plastic deformation mechanisms.[19] In particular, the strain prompting to failure is related to the H/E ratio, which analyzes the resistance to elastic deformation, whereas the H^3/E^2 ratio is related to the resistance to plastic deformation of thin films.[19,20] Summarizing, the higher the H/E ratio/index (higher elastic strain to failure), the higher the energy dissipation. Also, the higher the H^3/E^2 ratio/index (higher fracture toughness), the lower the energy dissipation. Thus, one must analyze both ratios to determine the real contribution of mechanical properties on the friction forces measured by NUS.

Figure 2 shows the H/E and H^2/E^3 indexes obtained by nanoindentation experiments for a-C:D/H thin films containing different [D]/[C] concentration ratios. One can see that the H/E indexes are quite the same within the experimental dispersion, showing that no energy dissipation is taking place by

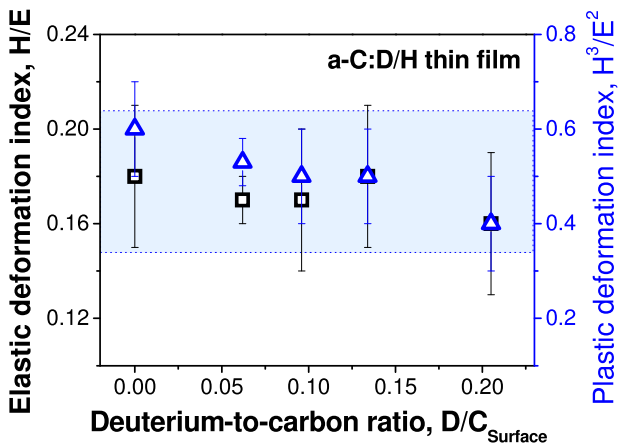

FIG. 2. H/E and H^2/E^3 indexes obtained by nanoindentation experiments for a-C:D/H thin films containing different [D]/[C] concentration ratios.

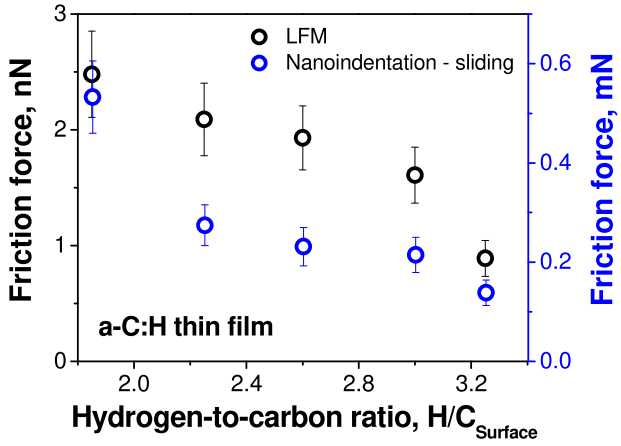

FIG. 3. Friction forces measured by NUS and LFM in a-C:H thin films having different [H]/[C] concentration ratios located at the outermost nanolayers of samples.

elastic deformation mechanisms. In the case of the H^2/E^3 index, this parameter slightly decreases with the increasing of the [D]/[C] ratio. Considering that a lower H^2/E^3 ratio would imply increasing energy dissipation by plastic deformation mechanisms which leads to the false interpretation of higher friction forces. Such behavior of the H^2/E^3 ratio goes in the opposite way and cannot explain the observed tendency.

To summarize this discussion, we understand that the friction forces measured by these two different techniques and scales (NUS and LFM) characterize the same physical phenomenon, i.e., a damping mechanism that is invariant from nanoscale to microscale and takes place at the outermost nanolayer due to dissipative friction forces. Indeed, a recent work has proposed for iron nitrides and oxides that the friction mechanism takes place at the outermost nanolayers, independently of magnetite thin film thicknesses, through phononic dissipation.[30]

To provide more experimental evidences to support the aforementioned results and conclusions, we have performed complementary experiments. Figure 3 shows the friction forces measured by NUS and LFM in a-C:H thin films having different [H]/[C] concentration ratios located at the outermost nanolayers. At the first glance, friction forces obtained by NFS and LFM techniques are different by orders of magnitude between them. However, we should note that the experimental results for a-C:H thin films behave similarly that the ones obtained for a-C: [D]/[H] thin films (Fig. 1). Therefore, as discussed above, one should compare the parameters H/E and H^2/E^3 to evaluate elastic and plastic

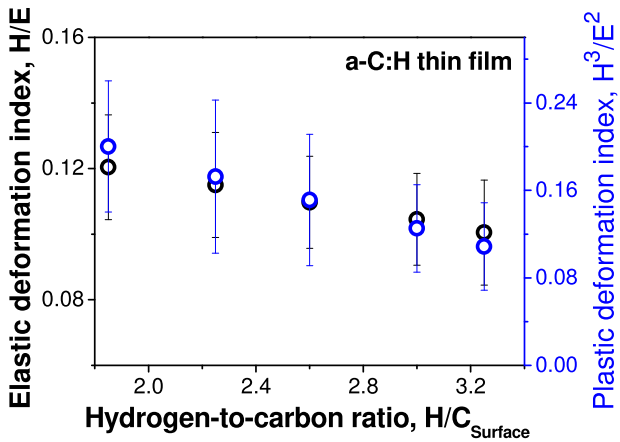

FIG. 4. H/E and H^2/E^3 indexes obtained by nanoindentation experiments for a-C:D/H thin films containing different [H]/[C] concentration ratios located at the outermost nanolayers of samples.

deformation mechanisms intervening in the experiments to have a complete picture of the physics involved in the phenomenon. Therefore, Figure 4 shows the H/E and H^2/E^3 indexes obtained for the a-C:H thin films by nanoindentation experiments at different [H]/[C] concentration ratios. The values for the indexes are within the experimental dispersion. Nevertheless, both indexes show a decreasing trend with the increasing of the [H]/[C] concentration ratio. Regarding the H^2/E^3 index ratio, the lower ratio, the higher the energy dissipation by plastic deformation mechanisms leading to higher friction forces. As aforementioned, such behavior goes in the opposite way of our experimental results and cannot explain the tendency shown in Fig. 3. In the case of the H/E index ratio, a lower ratio implies a lower energy dissipation by elastic deformation mechanisms. On the other hand, this trend is compatible with an energy dissipation phononic mechanism based on the wave propagation in elastic structures where a lower damping friction force is associated with a lower H/E index ratio.

A direct analysis by FEG-SEM in secondary electron mode of samples measured by the NUS technique provides more evidences supporting the above arguments. Figures 5(a)–5(c) show a sequence of FEG-SEM images after NUS measurements performed at high (500 mN) and low (10 mN) normal loads. Fig. 5a (top and yellow region) shows the trail performed by using a normal applied force of 500 mN. The plastic deformation (sink-in effect) of the a-C:H thin film is evident in the magnified micrograph (see Fig. 5b). Fig. 5a (bottom – blue region) also shows a region of the surface that suffered five sliding tests performed by applying a normal force of 10 mN, i.e., the same value used

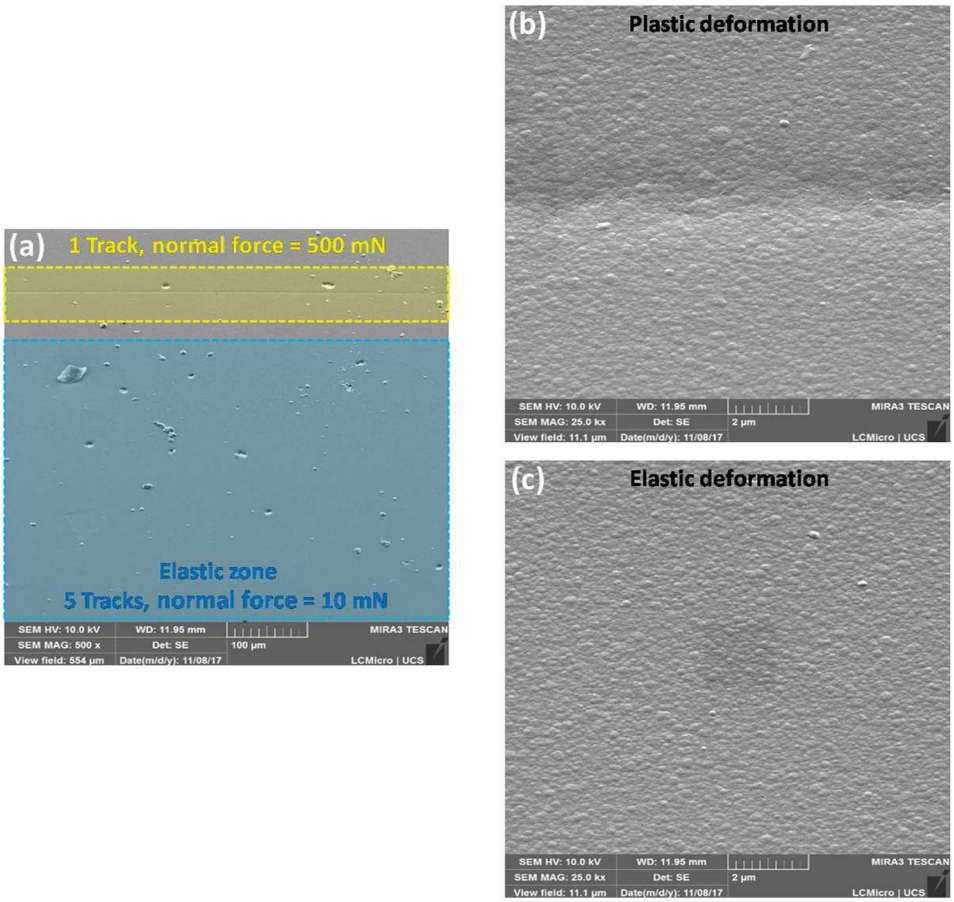

FIG. 5. (a) Scanning electron microscopy image in secondary electron mode and plain view (top and yellow region) where a trail was performed using a normal applied force of 500 mN. The plastic deformation (sink-in effect) of the a-C:H thin film is evident in the magnified micrograph (see (b)). At the bottom (blue region) is also shown a region of the surface that suffered five sliding tests performed applying a normal force of 10 mN. One can see that *no plastic* deformation mechanisms are apparent at this magnification (see (c)).

TABLE II. RMS surface roughness for different a-C:H/D and a-C:H thins films as measured by NUS and LFM.

	RMS surface roughness	
Sample ([D]/[C] ratio)	R_{NUS} (nm)	R_{LFM} (nm)
0	12 ± 3	0.50 ± 0.01
0.062	13 ± 3	0.48 ± 0.02
0.096	16 ± 2	0.57 ± 0.03
0.134	12 ± 3	0.55 ± 0.03
0.205	15 ± 3	0.51 ± 0.02
	RMS surface roughness	
Sample ([H]/[C] ratio)	R_{NUS} (nm)	R_{LFM} (nm)
1.85	26 ± 3	4.62 ± 0.07
2.25	27 ± 4	4.71 ± 0.08
2.60	27 ± 5	4.60 ± 0.07
3.00	27 ± 4	4.82 ± 0.10
3.25	24 ± 2	4.67 ± 0.07

in NUS friction experiments. One can see that *no plastic* deformation mechanisms are apparent at this magnification (Fig. 5c).

As we have proposed above, there are evidences that the friction behaviors established by the NUS and LFM techniques are scale-invariant (from nanoscale to microscale depending on contact area) and may have the same physical origin. According to phononic mechanisms invoked in dissipation energy phenomena at nanoscale sizes, the total damping friction force $F_{f,vib}$ coming from vibrational contribution is linearly proportional to the contact area, i.e., $F_{f,vib} = m_{tip}\eta v\sigma A$. Here $m_{tip,}$ is the mass of the tip; η, the friction coefficient; v, the tip sliding velocity; and A, the tip area of contact.[6] Thus, the higher the contact area between the sliding surfaces (i.e., tip and film), the higher the friction forces measured. Table II shows the surface roughness (RMS, root mean square) for all samples. The surface profiles and lateral force maps for NUS and LFM measurements can be found in Ref. 11, 15. Tables III and IV show the F_{NUS}/F_{LFM} (F = friction force) and A_{NUS}/A_{LFM} (A = contact area) ratios at different [D]/[C] and [H]/[C] ratios for a-C:D/H and a-C:H studied samples, respectively. The contact area ratio was determined considering that the AFM tip is a single asperity contact while the diamond tip is a multiple asperity contact (for further details, see Section III). If we analyze the A_{NUS}/A_{LFM} ratios, the contact areas for NUS experiments are ~ 5 (five) orders of magnitudes larger than for LFM experiments in both a-C: D/H and a-C:H thin film systems. In addition, the friction force ratios F_{NUS}/F_{LFM} obtained by the NUS and LFN techniques differ closely by ~ 5 (five) orders of magnitudes. What it is remarkable that this difference is understood by taking in account the ratio of the contact areas A_{NUS}/A_{LFM}, which are of the same order of magnitude. Thus, the two techniques yield equivalent friction forces if the ratio of the contact areas are considered. These small differences between friction force ratios and contact areas ratios (see Tables III and IV) come probably from a constant factor, which we attribute to a plastic deformation mechanism (not visible by FEG-SEM) and does not modify the general friction behavior. Thus, this convergence of values agrees with a scale-invariant friction mechanism from nanoscale to microscale. Also, the friction behavior evaluated by

TABLE III. Friction force ratios and contact area ratios at different D/C ratios in a-C:D/H thin films. The contact areas were calculated following the models explained in section III. We have used the real or effective contact area for ratios.

Sample ([D]/[C] ratio)	$F = F_{NUS}/F_{LFM}$	$A = A_{NUS}/A_{LFM}$	F/A
0	$4.0\text{x}10^5$	$1.2\text{x}10^5$	3.3
0.062	$4.3\text{x}10^5$	$1.2\text{x}10^5$	3.6
0.096	$4.0\text{x}10^5$	$1.2\text{x}10^5$	3.3
0.134	$7.6\text{x}10^5$	$1.2\text{x}10^5$	6.3
0.205	$8.2\text{x}10^5$	$1.2\text{x}10^5$	6.8

TABLE IV. Friction force ratios and contact area ratios at different H/C ratios in a-C:H thin films. The contact areas were calculated following the models explained in section III. We have used the real or effective contact area for ratios.

Sample ([H]/[C] ratio)	$F = F_{NUS}/F_{LFM}$	$A = A_{NUS}/A_{LFM}$	F/A
1.85	$2.1x10^5$	$3.4x10^5$	0.62
2.25	$1.3x10^5$	$3.4x10^5$	0.39
2.60	$1.2x10^5$	$3.2x10^5$	0.37
3.00	$1.3x10^5$	$3.3x10^5$	0.39
3.25	$1.5x10^5$	$3.3x10^5$	0.45

NUS and LFM may be associated with a damping mechanism through phonon coupling between the sliding surfaces.

A final comment. The hydrogenated and/or deuterated amorphous carbon thin films are smooth at nanoscale size, relatively hard, chemically inert and show super-low friction.[31,32] These properties could explain the scale-invariant friction behavior from nanoscale to microscale owing to friction forces depending manly on contact area.

V. CONCLUSIONS

Nanoindentation followed by unidirectional sliding and lateral force microscopy were used to measure the friction behavior of a-C:D/H and a-C:H thin films with different [D]/[C] and [H]/[C] concentration ratios, respectively. Surprisingly, the friction behavior assessed by these different techniques was the same in both thin films and friction forces differ in a constant factor. The H/E and H^2/E^3 indexes cannot explain the friction behavior through elastic and plastic deformation mechanisms. By considering that the AFM tip is a single asperity contact while the diamond tip is a multiple asperity contact, friction forces seem to depend mainly on a contact area factor, which may be originated in a quite similar physical phenomenon. We suggest that phononic dissipation mechanisms may explain the friction behavior. Finally, friction behaviors that depend mainly on contact area are scale-invariant (nanoscale to microscale) when elastic and plastic deformation mechanisms are not important to provide extra-friction. Such a scale-invariant friction behavior may open new understandings in connecting nanoscale and microscale friction measurements.

SUPPLEMENTARY MATERIAL

See supplementary material for the typical size of contact junctions from surface topographies and more details on contact mechanic parameters of thin films.

ACKNOWLEDGMENTS

This work is supported by the UCS, INCT-INES (# 465423/2014-0), FAPERGS. F.G.E., C.D.B., L.M.L., M.E.H.M.C., F.L.F.Jr, F.A. and C.A.F. are CNPq and CAPES fellows. S.R.S.M. is FAPERGS fellow. F.G.E. acknowledges support through of the Plasmar Tecnologia Ltda with sponsored Ph.D. studentship at the Universidade de Caxias do Sul. F.A. is indebted to FAPESP, project 2012/10127-5. The authors thank their colleagues and collaborators who participated in the preparation, testing, and characterization of the a-C:D/H and a-C:H thin films discussed in this work.

[1] D. Berman, A. Erdemir, and A. V. Sumant, ACS Nano **12**, 2122 (2018).
[2] J. Y. Park and M. B. Salmeron, Chem. Rev. **114**, 677 (2014).
[3] B. N. Persson, *Sliding friction: Physical Principles and Applications* (Springer-Verlag, 2000).
[4] S. J. Eder, G. Feldbauer, D. Bianchi, U. Cihak-Bayr, G. Betz, and A. Vernes, Phys. Rev. Lett. **115**, 025502 (2015).
[5] J. Krim, Adv. Phys. **61**, 155 (2012).
[6] R. Kubo, Rep. Prog. Phys. **29**, 255 (1966).
[7] R. J. Cannara, M. J. Brukman, K. Cimatu, A. V. Sumant, S. Baldelli, and R. W. Carpick, Science **318**, 780 (2007).
[8] A. Bylinskii, D. Gangloff, and V. Vuletić, Science **348**, 1115 (2015).
[9] J. Zekonyte and T. Polcar, ACS Appl. Mat. & Interf. **7**, 21056 (2015).
[10] C. M. Mate, G. M. McClelland, R. Erlandsson, and S. Chang, Phys. Rev. Lett. **59**, 1942 (1987).

[11] S. R. Sales de Mello, M. E. H. Maia da Costa, C. M. Menezes, C. D. Boeira, F. L. Freire, Jr., F. Alvarez, and C. A. Figueroa, Scientific Reports **7**, 3242 (2017).
[12] M. Freislebem, C. M. Menezes, F. Cemin, F. B. Costi, P. A. Ferreira, C. Aguzzoli, I. J. R. Baumvol, F. Alvarez, and C. A. Figueroa, Appl. Phys. Lett. **105**, 111603 (2014).
[13] M. E. H. Maia da Costa and F. L. Freire, Jr., Surf. Coat. Technol. **204**, 1993 (2010).
[14] S. M. M. Dufrène, F. Cemin, M. R. F. Soares, C. Aguzzoli, M. E. H. Maia da Costa, I. R. J. Baumvol, and C. A. Figueroa, Applied Physics A **117**, 1217 (2014).
[15] F. G. Echeverrigaray, S. R. S. de Mello, L. M. Leidens, M. E. H. Maia da Costa, F. Alvarez, T. A. L. Burgo, A. F. Michels, and C. A. Figueroa, Phys. Chem. Chem. Phys. **20**, 21949 (2018).
[16] E. R. Petry, C. D. Boeira, F. Cemin, L. M. Leidens, L. T. Bim, D. G. Larrude, M. E. H. Maia da Costa, and C. A. Figueroa, Surf. Eng. **32**, 779 (2016).
[17] D. F. Ogletree, R. W. Carpick, and M. B. Salmeron, Rev. Sci. Instrum. **67**, 3298 (1996).
[18] W. C. Oliver and G. M. Pharr, J. Mater. Res. **7**, 1564 (1992).
[19] A. Leyland and A. Matthews, Wear **246**, 1 (2000).
[20] K. L. Johnson, *Contact Mechanics* (Cambridge University Press, 1985).
[21] H. Hertz, J. Reine Angew. Math. **92**, 156 (1881).
[22] K. L. Johnson, Proc. R. Soc. Lond. A **453**, 163 (1997).
[23] J. A. Greenwood and J. B. P. Williamson, Proc. R. Soc. Lond. A **295**, 300 (1966).
[24] J. A. Greenwood and J. H. Tripp, J. Appl. Mech. **34**, 153 (1967).
[25] A. Kapoor, J. A. Williams, and K. L. Johnson, Wear **175**, 81 (1994).
[26] B. Bhushan, J. Tribol. **106**, 26 (1984).
[27] F. P. Bowden and D. Tabor, Brit. J. Appl. Phys. **17**, 1521 (1966).
[28] L. Pastewka and M. O. Robbins, Appl. Phys. Lett. **108**, 221 (2016).
[29] M. H. Müser, Tribol. Lett. **64**, 14 (2016).
[30] N. Bogoni, Jr., C. M. Menezes, F. B. Costi, B. L. Perotti, F. G. Echeverrigaray, C. A. Perottoni, F. Alvarez, and C. A. Figueroa, Thin Solid Films **660**, 258 (2018).
[31] J. Robertson, Mater. Sci. Eng. R: Reports **37**, 129 (2002).
[32] H. Ronkainen, S. Varjus, and K. Holmberg, Surf. Coat. Technol. **249**, 267 (2001).